ELECTRONIC STRUCTUREELECTRONIC STRUCTURE OF LIQUID AND AMORPHOUS METALS

H. Güntherodt, P. Oelhafen, R. Lapka, H. Künzi, G. Indlekofer, J. Krieg, T. Laubscher, H. Rudin, U. Gubler, F. Rösel, et al.

ELECTRONIC STRUCTURE.

ELECTRONIC STRUCTURE OF LIQUID AND AMORPHOUS METALS

H.J. Güntherodt, P. Oelhafen, R. Lapka, H.U. Künzi, G. Indlekofer, J. Krieg, T. Laubscher, H. Rudin, U. Gubler, F. Rösel, K.P. Ackermann[1], P. Delley[2], M. Fischer[3], F. Greuter[4], E. Hauser[5], M. Liard[6], M. Müller[7], J. Kübler[+], K.H. Bennemann[++] and C.F. Hague[+++].

Institut für Physik, Universität Basel, CH-4056 Basel, Switzerland
[+]Physik-Institut, Ruhr-Universität, D-4630 Bochum, R.F.A.
[++]Theoretische Physik, Freie Universität Berlin, D-1 Berlin 33, R.F.A.
[+++]Laboratoire de Chimie Physique, Université Pierre et Marie Curie, F-75031 Paris, France

Note : The authors have included in this review the presentation of two of their posters.

1. INTRODUCTION - This paper will review the progress made in understanding the electronic structure of liquid (ℓ) and amorphous (a) metals since the Bristol conference. Today, because we know how to explain the properties of simple ℓ- and a-metals and their alloys by the pseudopotential approach, the interest has shifted more towards transition (T) and rare earth (RE) metals and their alloys. Many of the known alloy groups which form metallic glasses (MG's) contain T and RE: T-N (e.g. $Fe_{80}B_{20}$); T_E-T_L (e.g. $Pd_{35}Zr_{65}$); RE-N (e.g. $La_{70}Al_{30}$) and RE-T (e.g. $Gd_{70}Co_{30}$), where N: polyvalent metal, T_L: late and T_E: early transition metal.

Until quite recently information about the electronic structure of ℓ- and a-metals and their alloys has been primarily deduced from their electronic transport and magnetic properties. These experiments were very helpful in establishing for at least these properties a strong similarity between the liquid and glassy (g) states. The recent experimental results on the electrical resistivity, the thermopower and the Hall coefficient are reviewed and contrasted with theoretical explanations.

The most direct experimental techniques such as electron and optical spectroscopy in terms of photoemission (Ultraviolet Photoemission Spectroscopy: UPS, X-Ray Photoemission Spectroscopy: XPS) experiments on valence bands, X-ray core level spectroscopy, Auger Electron Spectroscopy (AES) and optical reflectivity are difficult to apply to ℓ-samples and a-films at low temperatures. Only recently the MG's have opened a new field for systematic studies of the electronic structure of glassy metals containing T and RE. We review the available photoemission data and concentrate on MG's of the group T_E-T_L. For these alloys systematic studies of UPS

Present address : [1]BBC, Baden
[2]Northwestern University, Evanston Ill., U.S.A.
[3]BBC, Dättwil
[4]University of Pennsylvania, Philadelphia, U.S.A.
[5]Balzers AG, Balzers
[6]F. Hoffmann-la Roche & Co. AG, Basel
[7]Gretag AG, Regensdorf

and X-ray core level spectroscopy are available. Additional information comes from Soft X-ray Spectroscopy (SXS). Detailed calculations of the realistic band structure for the corresponding crystalline compounds by the ASW (Augmented Spherical Waves) method (1) provide an excellent insight into the subject of the round table discussion "Electronic Structure versus Atomic Scale Structure" at this meeting.

2. ELECTRICAL TRANSPORT PROPERTIES - The experimentally observed magnitude, as well as temperature and composition dependence of the electrical resistivity of ℓ- and g-metals at high temperatures ($T \geq T_D$; where T_D: Debye temperature) are comparable. In ℓ- and g-metals and alloys it is often found that the resistivity decreases with increasing temperature. Such negative temperature coefficients (NTC's) in the ℓ-state have traditionally been explained by the Ziman theory. This theory deals with the potential scattering of the conduction electrons by a disordered array of scattering centers. In simple ℓ-metals these scattering centers have been represented by pseudopotentials, and in ℓ-T and RE metals by muffin-tin potentials. Subsequently, the Ziman theory has been extended to explain the NTC's in ℓ-RE and in alloys of ℓ-T and RE metals. A NTC can be obtained in this model if $2k_F \sim k_p$, where k_p is the position of the first peak in the structure factor S(k) and $2k_F$ is the diameter of the Fermi sphere.

The original Ziman theory was essentially a weak scattering theory and it is not clear that it should be valid for such strong scattering materials as ℓ-T and RE metals. In these cases the resistivity is very high and the mean free path very short. Clearly a crucial test of this theory would be an explanation of the resistivity of the divalent metals Eu, Yb and Ba which have $2k_F \sim k_p$. The successful application of this theory to ℓ-RE and their alloys (2,3, 4) shows that the Ziman approach appears to be valid even outside the weak scattering regime for which it was originally indended. Moreover, such an application gives evidence for varying d-band occupancy across the trivalent RE series in accord with band structure calculations, thus providing information about the number of s,p and d electrons which contribute to the total number of three valence electrons for the RE.

The electrical resistivity and its temperature coefficient for the ℓ-RE series show the following behaviour: For the trivalent elements the resistivity increases rather monotonically from La to Lu, whereas the temperature coefficient changes from slightly positive at La to slightly negative at Lu. Those elements which are divalent, i.e. Eu and Yb, behave exceptionally: for Eu the resistivity is higher than for any element of the RE series, whereas Yb has a very low value. In both cases the temperature coefficient is negative. The key quantity is the number

of conduction electrons per ion. For Eu and Yb two conduction electrons are assumed, whereas bandstructure calculations (5) for the RE's give evidence that, for the trivalent elements, the number of conduction electrons increases from about 0.5 for La to 1.5 for Lu. These facts explain the trend of the resistivity and its temperature coefficient for the ℓ-RE series. Particularly, the $2k_F$ values calculated for Eu, Yb and Lu are very close to the corresponding k_p values. Detailed quantitative calculations of the electrical resistivity and its temperature coefficient for ℓ-Eu, Yb, La, Gd and Lu are in good agreement with experimental results (3,4).

In view of the strong similarities of the ionic and electronic properties of the ℓ- and g-states, the extended Ziman theory was used as a first starting point to understand the resistivity of MG's. In the meantime a more general formalism was developed to describe the resistivity in the range $T<T_D$ (6). Indeed, many of the recently studied MG's show NTC's. Among these systems are alloys of the T_E-T_L, RE-N and RE-T groups. All these alloys show NTC's in the ℓ-state. In order to fulfill the condition $2k_F \sim k_p$ the following conclusions can be drawn: The T_E provide two or even more conduction electrons per atom, in any case more than the T_L. The NTC's of g-La-Aℓ alloys can be explained in a similar way as for liquid Ce-Sn. A possible breakdown of the Ziman model might be indicated by the NTC's in g- and ℓ- RE-T alloys. The apparent inconsistency can only be replaced by the fact, that $2k_F$-values of the alloys cannot simply be extrapolated from the values of the pure components. Charge transfer can alter these numbers. Moreover, the reported NTC's of g- Au-La are the strongest evidence against the Ziman approach. However, the liquid alloys of the monovalent noble metal-RE alloys show positive temperature coefficients. As examples the electrical resistivity of g- and ℓ-$Gd_{67}Co_{33}$ and of glassy alloys of Zr are shown in Figs. 1 and 2. The observed resistivity values of the g-Zr alloys are by a factor of two smaller than reported in the literature (7,8).

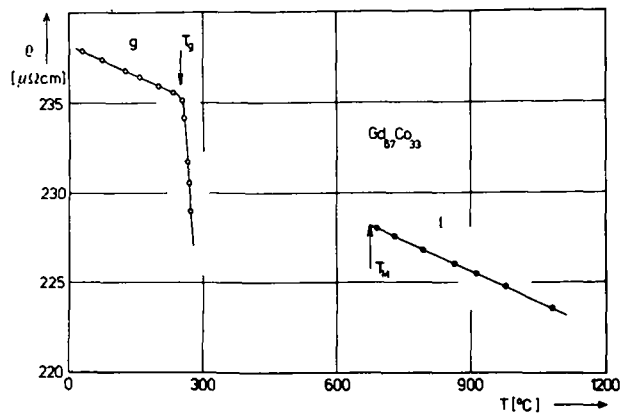

Fig.1 Resistivity of liquid and glassy $Gd_{67}Co_{33}$

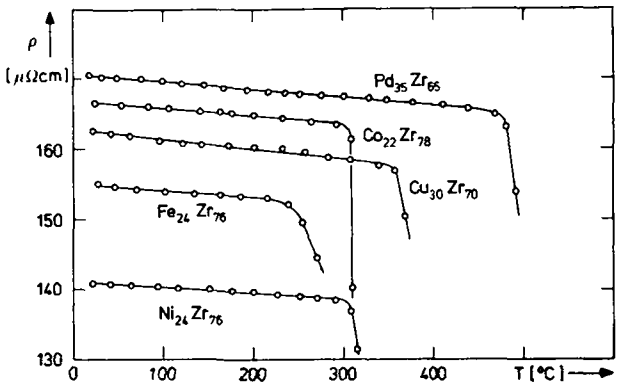

Fig.2 Resistivity of glassy alloys of Zr.

Several other theories have attempted to explain the NTC's of MG's. For a recent review see Ref.9. Unfortunately, it is very difficult to produce actual numbers of the resistivity and its temperature coefficient by these alternative theories. Therefore, it is still considerable controversy which of these theories is most applicable for explaining the experimental results. An alternative theory (10,11) proposes the existence of quantum-mechanical two-level states for some atoms in a disordered solid. The scattering of electrons from the localized excitations arising from these tunneling states can give rise to both a resistivity minimum and a NTC over a wide temperature range. Another theory proposed to explain the NTC's is the Mott s-d scattering model (12) which relates the NTC's to the density of states at the Fermi energy E_F. Of similar origin is the idea given by Brouers (13). In view of the now available photoemission data it would be very attractive to examine these models again. Finally, a recent theory by Johnson and Girvin (14) which relates the NTC's to localization phenomena is of particular interest. They suggest a microscopic origin of the Mooij correlation in terms of a strong scattering theory. The Mooij correlation (15) says that systems with resistivity larger than 150μΩcm generally have NTC's. In order to decide how suited the Jonson and Girvin idea is to understand the resistivity in ℓ- and g-metals, it would be extremely helpful to know the consequences of this theory for the thermopower and for the Hall coefficient.

The study of the thermoelectric power is particularly valuable to test theories of the electrical resistivity since it is given by the energy derivative of the resistivity. Therefore, measurements of the thermoelectric power can identify the scattering mechanism which most accurately describes the electrical transport in the liquid and glassy states. Furthermore, the predicted behaviour of the thermoelectric power by the various models will be substantially different. For the non-magnetic MG's, it is apparent that of the existing theories only the Ziman theory is consistent with the experimental thermoelectric power results. In this theory the thermopower should be a linear function of temperature with a small slope. The thermoelectric power will be positive if $2k_F \sim k_p$. For those alloys with a NTC it was found that the thermopower was small, positive, and varied linearly with temperature over the entire range from 10K to 600K. (See Ref.16).

The Hall coefficients of g- Mg-Zn and Pd-Si alloys show a negative sign and seem to be in reasonable agreement with the free-electron model. However, many of the studied MG's show positive Hall coefficients. More details are shown in Table 1. It becomes obvious that the positive Hall coefficients of the glassy alloys are related to the positive values of the pure components dominating the electronic

transport. Positive Hall coefficients were observed for pure Fe, Co, La and Ce in the liquid state. There is still no satisfactory theory to explain such positive Hall coefficients. Mott's idea (17) concerning the Hall effect in non-crystalline systems has still to be extended to ℓ- and g-metals. The shifts of the Hall coefficients of Pb and Bi towards smaller values as compared to the free-electron model have been explained in terms of skew scattering due to the spin-orbit interaction (18). This theory has been extended to ℓ-T metals (19) in terms of exchange scattering. Although the effect of exchange scattering is an order of magnitude larger than that of spin-orbit scattering, it is still an order of magnitude too small to account for the Hall coefficient of ℓ- Fe and Co.

Table 1 Hall coefficient of several MG's at room temperature.

ALLOY	$Mg_{70}Zn_{30}$	$Pd_{81}Si_{19}$	$Cu_{30}Zr_{70}$	$Cu_{45}Zr_{55}$
$R_H\left[10^{-11}\frac{m^3}{As}\right]$	-8.3	-9.6	+7.3	+8.7
ALLOY	$Cu_{60}Zr_{40}$	$Cu_{50}Ti_{50}$	$Ni_{24}Zr_{76}$	$Co_{22}Zr_{78}$
$R_H\left[10^{-11}\frac{m^3}{As}\right]$	+6.6	+12	+2.5	+2.4
ALLOY	$Fe_{24}Zr_{76}$	$La_{70}Al_{30}$	$La_{65}Co_{35}$	$Sm_{65}Co_{35}$
$R_H\left[10^{-11}\frac{m^3}{As}\right]$	+4.1	+9.6	-9.0	-10.6

We have measured the Hall coefficients of paramagnetic $(Fe_xNi_{1-x})_{77}B_{13}Si_{10}$ alloys (x: 0-15 at.%) in order to reveal more information about the Hall effect in g-metals. The main aim has been to study the change of sign from negative to positive. The measured Hall coefficients ranging from $-8.72 \cdot 10^{-11}$ m³/As for Ni-rich alloys to $+30.5 \cdot 10^{-11}$ m³/As for alloys containing more Fe. Figure 3 shows a summary of the measured Hall coefficients R_H at 20 and 200°C, the normal Hall coeffient R_0, the resistivity and its temperature coefficient as a function of Fe concentration. In the paramagnetic region the measured Hall coefficient R_H is given by $R_H = R_0 + R_1 \chi$, where R_1 is the anomalous Hall coefficient.

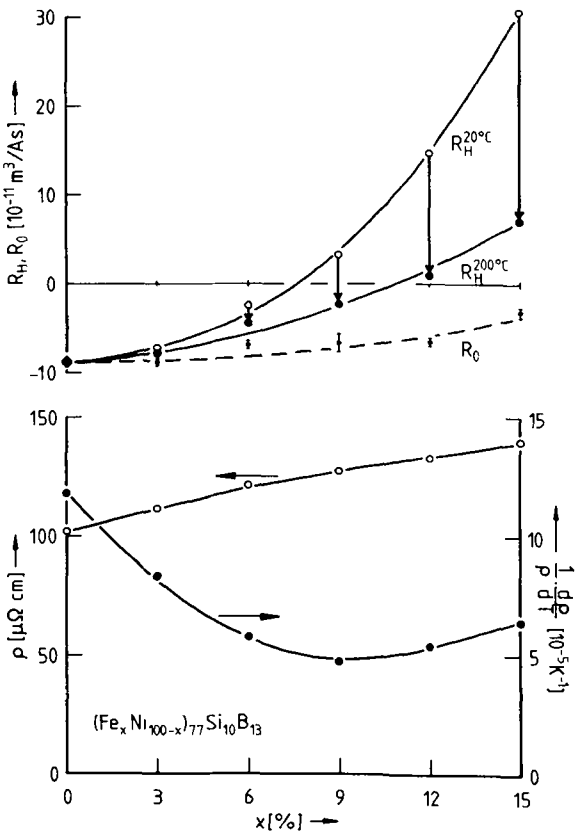

Fig.3 Measured Hall coefficient R_H at 20 and 200°C, normal Hall coefficient R_0, electrical resistivity and its temperature coefficient of glassy $(Fe_xNi_{1-x})_{77}B_{13}Si_{10}$.

Therefore, the normal Hall coefficient R_0 can be separated from the total R_H by

plotting R_H versus χ, the magnetic susceptibility. The Hall coefficients at 20 and 200°C and the normal Hall coefficient change from negative to positive with increasing Fe concentration. Such a change of sign is already indicated in ℓ-$(Fe_xNi_{1-x})_{80}Ge_{20}$ alloys (20).

3. ELECTRON SPECTROSCOPY - A comparison of the electronic density of states of ℓ- and g- metals and alloys with the density of states in the crystalline state yields information on the role of crystal periodicity on the electronic states. Moreover, the density of states is the key for the explanation of many physical properties such as magnetism, superconductivity, compound formation etc. Furthermore, the relationship between the electronic band structure and the atomic scale structure on the one hand and the glass forming ability on the other hand is of great interest.

The following metallic glasses have been studied by photoemission: $Pd_{77.5}Cu_6Si_{16.5}$ (21), Pd-Si (22-24), $Fe_{80}B_{20}$ and similar alloys (25-27), and alloys of the following two groups: RE-T (27) and T_E-T_L (28-32).

The most comprehensive and exciting results on the MG's so far studied come from alloys containing T_E and T_L. The investigated alloys are: Fe-Zr, Co-Zr, Ni-Zr, Cu-Zr, Pd-Zr, Pt-Zr, Rh-Zr, Cu-Ti, Ni-Nb and Ni-Ta. Figure 4 shows the valence band spectra of glassy alloys of Zr with Cu, Pd, Ni, Co and Fe. All these spectra are

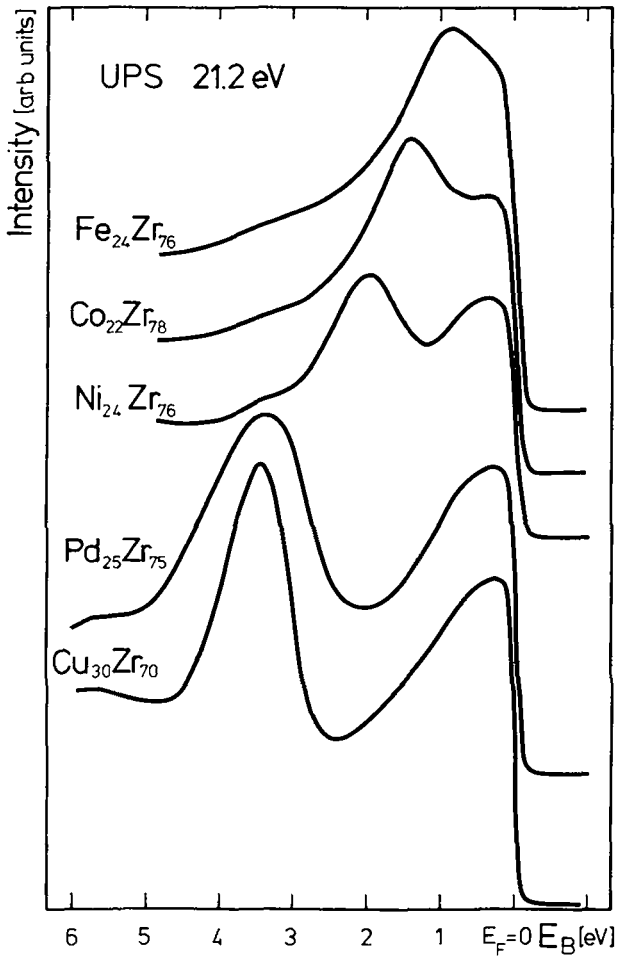

Fig.4 Valence band spectra of alloys of Zr with Cu,Pd,Ni,Co and Fe obtained by UPS.

characterized by varying d-band splittings and binding energy shifts. There is a distinct two peak structure of Cu and Pd alloys with Zr. In other words, the valence bands of these two alloys are formed by two well separated components, one lying close to the Fermi energy E_F, the other appearing at a higher binding energy. The relative intensities of the two peaks are modified as the relative composition of the alloy is changed, from which it is concluded that the Pd 4d- and Cu 3d-bands have shifted from their positions relative to E_F in the pure metal. The T_L d-states

provide the main contribution to the higher binding energy component of the spectrum. Such a behaviour is in contrast to the results of solid solutions e.g. Cu-Ni, Ag-Pd, but is typical for crystalline intermetallic compounds (33,34). The separation of the two d-band peaks is decreased by replacing Cu and Pd by Ni, Co and Fe. From measurements performed at different alloy compositions it was established that the high binding energy peak in Ni-Zr, Co-Zr and the maximum in the Fe-Zr spectrum is mainly related to d-states of the late transition metal and the peak near E_F to the Zr d-states.

The shift of the d-states of T_L to higher binding energies results in a decrease of the local density of states at E_F for the T_L. Since the core level line shape is related to the local density of states near E_F, the core level line shapes of the T_L, which are highly asymmetric in the pure metals, become very symmetric in the glassy alloys. (Fig.5).

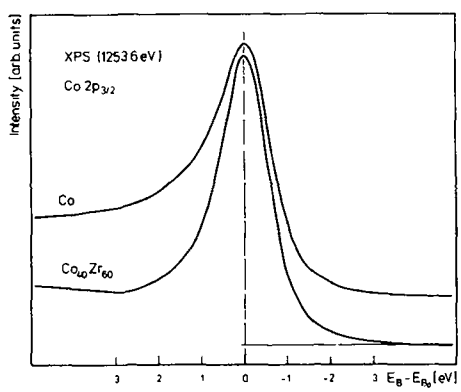

Fig.5 Core level line shapes of Co $2p_{3/2}$ in the pure metal and in the glassy alloy $Co_{40}Zr_{60}$.

A comparison of the photoemission spectra for the MG's $Pd_{35}Zr_{65}$ and $Cu_{60}Zr_{40}$ with the corresponding result for the crystalline compounds $PdZr_2$ and Cu_3Zr_2 shows that the d-band splitting and d-band binding energy shift is not a specific property of the glassy alloys but is also found in the crystalline phase. We find essentially the same d-band peak positions for Pd and Cu in the crystalline and glassy state. However, the shape of the d-band is changed. In the crystalline compound Cu_3Zr_2 (Fig.6) the Cu d-band peak exhibits the covalent splitting which is typical of the pure Cu d-band spectrum, whereas in the glassy state the Cu d-band becomes more Gaussian-like.

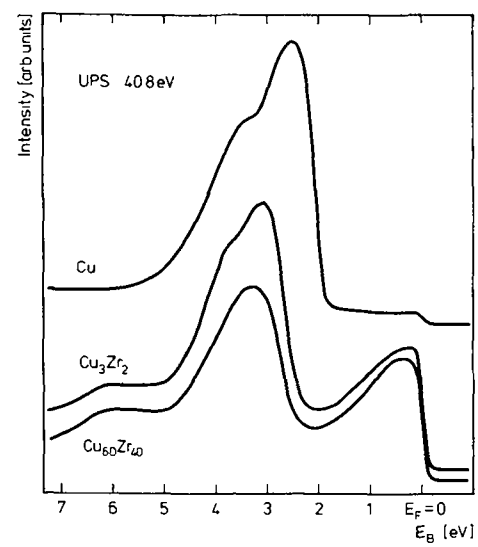

Fig.6 UPS spectra of pure Cu, the crystalline compound Cu_3Zr_2 and the glassy alloy $Cu_{60}Zr_{40}$.

The strong similarity of the d-band positions in the crystalline and glassy state has two important consequences:

1. For the positions of the d-bands realistic calculations for crystalline compounds

can be used to gain insight into the position of the d-band in the crystalline as well as in the glassy state.

2. The alloy heats of formation are mainly determined by the d-band position and width. Therefore, the heat of formation for the g-state is only slightly different from the one of the crystalline state. This fact is supported by measurements of heats of crystallization which turned out to be small compared to the alloy heats of formation. This means that the g-state lies energetically very close to the crystalline state. Consequently, the question arises what determines for a given composition whether a crystalline compound or a MG is formed?

Recent band structure calculations (35) for crystalline compounds using the ASW method are consistent with our results and reproduce the observed trends. Williams et al. (36) calculated the density of states for a crystalline Zr-Rh compound. These results for the crystalline state show considerable structure in the d-bands. The first calculations for these systems based on the amorphous structure are presented at this conference (37,38).

Figure 7 shows the total (s,p,d) and the partial d-density of states calculated by the ASW method in comparison with the experimental UPS data of glassy $Pd_{25}Zr_{75}$. The calculated results refer to the crystalline compound $PdZr_3$ with Cu_3Au type symmetry. The partial d-density of states indicates a splitting of the Pd and Zr

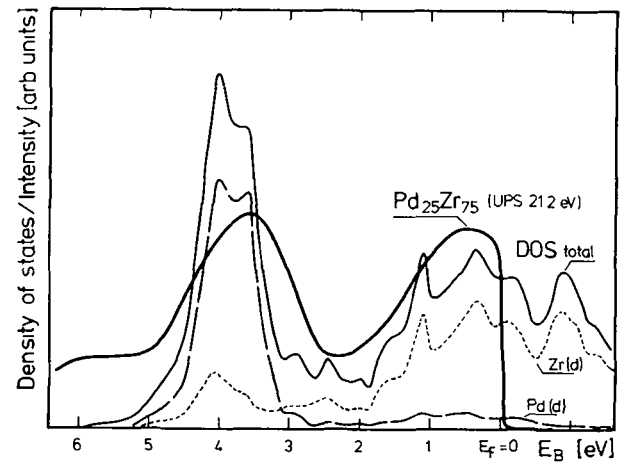

Fig.7 Calculated total (s,p,d) and partial d-density of states DOS of the crystalline compound $PdZr_3$ with Cu_3Au symmetry and the UPS spectrum of glassy $Pd_{25}Zr_{75}$.

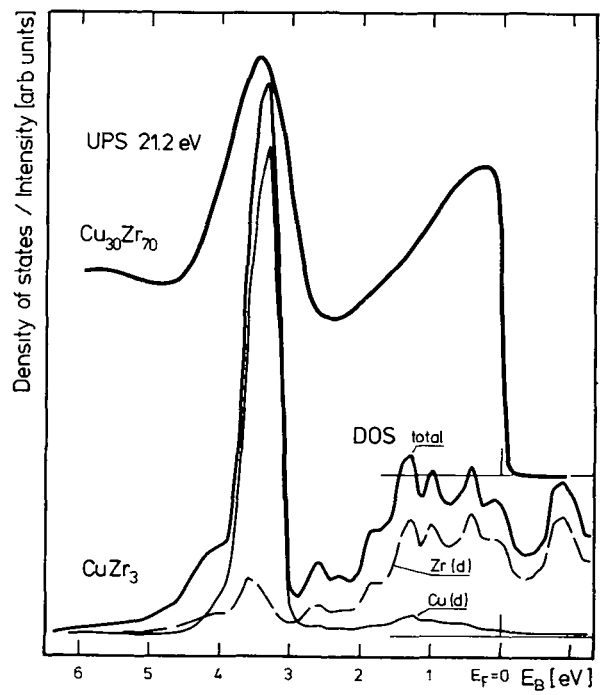

Fig.8 Calculated total (s,p,d) and partial d-density of states of the crystalline compound $CuZr_3$ with Cu_3Au symmetry and the UPS spectrum of glassy $Cu_{30}Zr_{70}$.

states itself in order to build up the two peak structure. Again this behaviour is in strong contrast to what is known for solid solutions. Figure 8 shows similar data for

the crystalline compound $CuZr_3$ and the glassy $Cu_{30}Zr_{70}$ alloy. Another example shows the band structure calculation of a NiNb compound. (Fig.9). The d-band complex is shifted closer to E_F when the CuAu- or CsCl-structure is applied instead of the NaCl-structure. For comparison the partial d-density of states for Ni is shown. It is clearly seen that the peak at 1.2eV in the UPS spectrum arises from Ni d-states. Therefore the Ni d-band is significantly shifted to higher binding energies relative to pure Ni.

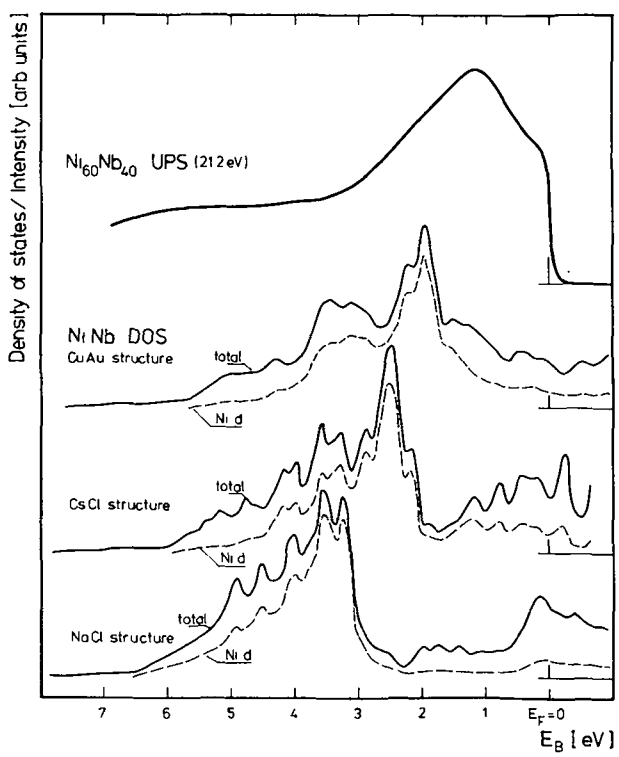

Fig.9 Calculated total (s,p,d) density of crystalline NiNb with NaCl, CsCl and CuAu structure and the UPS spectrum of glassy $Ni_{60}Nb_{40}$. For comparison the partial Ni d-densities of states are shown.

Photoemission experiments yield only the total density of states and are not capable of distinguishing between d-states coming from Pd and Zr. Therefore, SXS experiments (39) have been performed to probe the local electronic structure by determining the partial d-density of states.

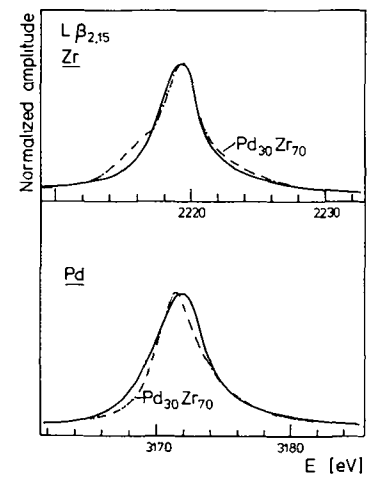

Fig.10 The Pd and Zr SXS $L\beta_{2,15}$ emission bands in the pure metals and in glassy $Pd_{30}Zr_{70}$.

Figure 10 shows the Pd and Zr $L\beta_{2,15}$ X-ray emission bands in the pure metals and in glassy $Pd_{30}Zr_{70}$. Indeed, this experiment supports the results of the above mentioned calculations and the results obtained by electron spectroscopy. The $L\beta_{2,15}$ emission band of Zr in the alloy shows on the low energy side a shoulder confirming the splitting of the Zr d-band. In solid solutions such a shoulder does not occur (40). The $L\beta_{2,15}$ emission band of Pd in the alloy shows a shift to lower energies with respect to pure Pd. A very similar spectrum as obtained by UPS can be constructed by positioning the X-ray emission bands with respect to E_F by means of X-ray core level binding energy determinations. These

experimental results are in good agreement with recent cluster calculations (37,39).

There are two interesting correlations between 1.) the glass forming ability, the glass temperature and the d-band binding energy shift E_B of the T_L, and 2.) the glass forming ability and the alloy heats of formations of this alloy group. For more details see Ref.35 .

There is still the open question, to what extent the Pd d-electrons contribute to the density of states at E_F in glassy Pd-Si (22,23). In view of the successful application of the ASW method to T_E-T_L alloys, we performed calculations for crystalline Pd_3Si in the Cu_3Au structure. The calculations are shown in Fig.11 and compared with the UPS spectrum of glassy $Pd_{84}Si_{16}$. The partial d-density of states is given per Pd atom and therefore their contribution to the total density of states has to be multiplied by a factor of three. Note, that the main contribution to the density of states at E_F is coming from Pd d-states.

We would like to include very recent data on a specific topic of electron spectroscopy which goes beyond the single partial picture used in photoemission and in band structure calculations. The subject deals with the Secondary Electron Emission (SEE) and the Energy Loss Spectroscopy (ELS) in the liquid state. Figure 12 shows a typical electron spectrum obtained by bombarding solid and liquid Hg with electrons having a primary energy of 25eV. The

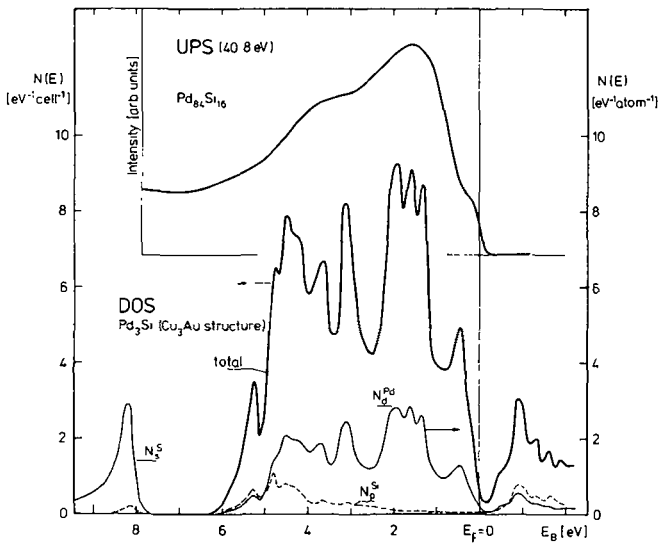

Fig.11 The calculated total and partial density of states of Pd_3Si in the Cu_3Au structure and the UPS spectrum of glassy $Pd_{84}Si_{16}$.

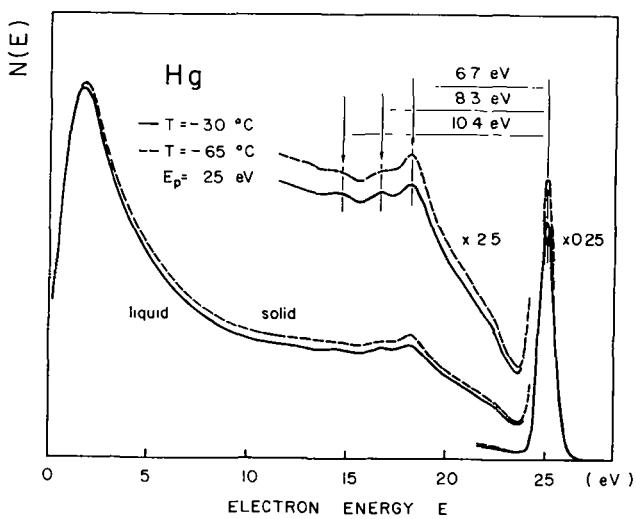

Fig.12 Secondary electron emission and electron energy loss spectra of solid and liquid Hg.

part of the spectrum in the energy range 0 to 10eV is typical of a SEE spectrum. The range from 15 up to 25eV shows a typical electron energy loss spectrum. The observed structures can be explained in the following way: The peak at 6.7eV arises from

volume plasmon excitation. The structures at 8.3 and 10.4eV can be attributed to interband transitions to E_F from the Hg $5d_{3/2,5/2}$ -states which are located at binding energies of 8 and 10eV respectively (41). These three structures do not change at the solid-liquid transition. However, the SEE spectra in the solid and liquid states are slightly different, probably reflecting the difference in the surface properties. Figure 13 shows the electron energy loss spectrum and its second derivative for liquid Ga. The two intense energy loss peaks at 10.7 and 14.2eV can be explained by surface and volume plasmon excitations. The weaker structures in the range of 20 to 30eV can be attributed to combined surface and volume plasmon losses. These plasmon excitations are reflected in SEE spectra. Due to plasmon decay a single electron from the valence band can be excited and will contribute to the secondary electron intensity (42). The kinetic energy of such an excited electron is given by $E_{kin} \leq \hbar\omega - \phi$, where $\hbar\omega$ is the plasmon energy and ϕ is the work function of the liquid sample (42). Figure 14 shows the SES data of liquid Ga and Hg, where we observe such contributions for Ga, but not for Hg. In the case of liquid Ga ($\phi = 4.3$eV; $\hbar\omega = 10.7$ and 14.2eV) the maximum kinetic energy of an excited secondary electron is 6.4eV, due to surface plasmon decay, and 9.9eV, due to volume plasmon decay. By taking into account the work function of the retarding field analyzer

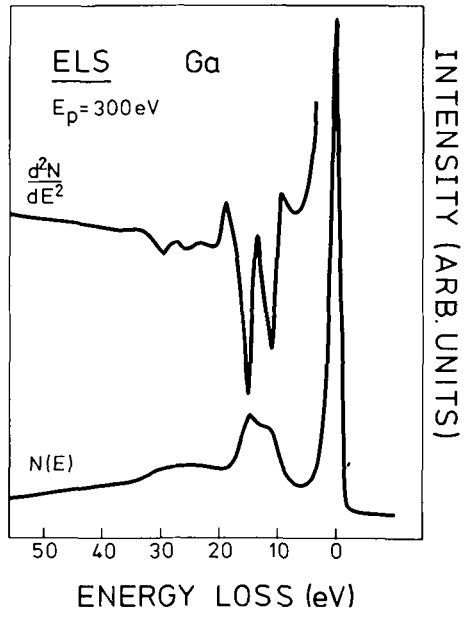

Fig.13 Electron energy loss spectrum and its second derivative of liquid Ga.

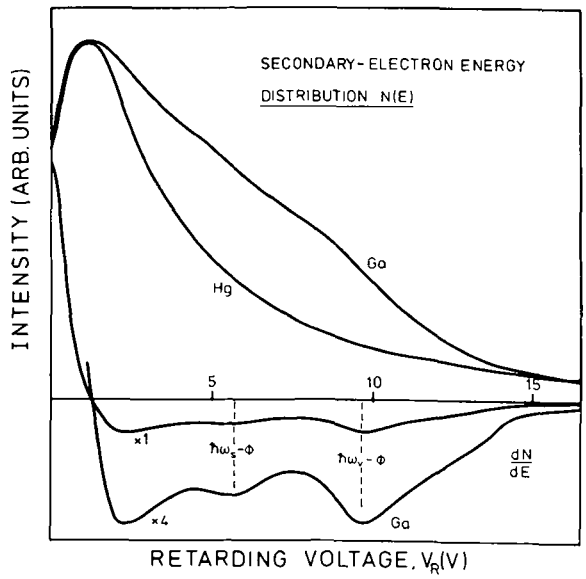

Fig.14 Secondary electron energy distribution and its derivative.

these two limits appear at 6.2 and 9.7eV as shown by the dashed lines in Fig.14. In the case of Hg ($\phi = 4.5$eV, $\hbar\omega = 6.7$eV) the electrons due to plasmon decay can only occur below an energy of 2.2eV and therefore coincide with the maximum of the

SEE distribution.

4. OPTICAL PROPERTIES

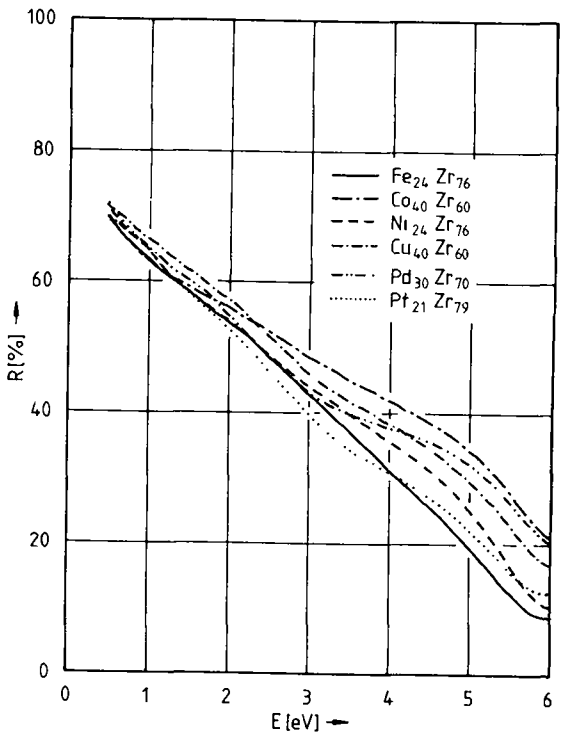

Fig.15 Optical reflectivity of glassy alloys of Zr with Cu,Pd,Pt,Ni,Co and Fe.

The experimental results obtained by electron spectroscopy can be supported by optical spectroscopy. This has been shown for Pd-Si glasses (44). Here, the main emphasis is on the alloys of group T_E-T_L. Figure 15 shows the optical reflectivity data of alloys of Zr with Cu, Pt, Pd, Ni, Co and Fe. The reflectivity of pure Zr is very close to the one of $Fe_{24}Zr_{76}$. Certainly for a detailed discussion a Kramers-Kronig analysis has to be prepared and the optical reflectivity data of the pure components have to be taken into account. Most clearly a relation between the density of states and the optical reflectivity is seen by a comparison of the data of glassy $Pd_{30}Zr_{70}$ and $Fe_{24}Zr_{76}$. Figure 16 shows the optical reflectivity of glassy $Pd_{30}Zr_{70}$. There is a structure at approximately 4eV which is also the binding energy of the Pd d-states.

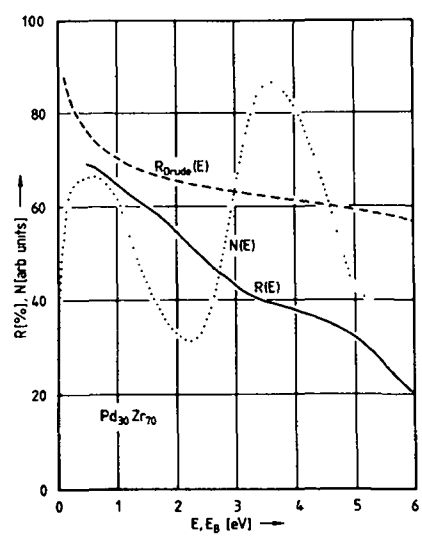

Fig.16 Optical reflectivity of $Pd_{30}Zr_{70}$ and comparison with UPS spectra and Drude theory.

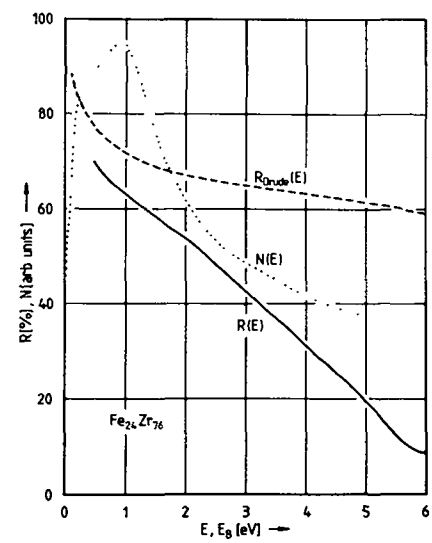

Fig.17 Optical reflectivity of $Fe_{24}Zr_{76}$ and comparison with UPS spectra and Drude theory.

The UPS spectrum is drawn on the same figure to illustrate this point. We therefore associate this structure in the reflectivity with transitions from the Pd d-states to E_F. The optical reflectivity and the UPS spectrum of $Fe_{24}Zr_{76}$ is shown in Fig.17 . In contrast to Fig.16 the optical reflectivity does not show any structure around 4eV.

Measurements of the optical reflectivity were extremely helpful to elucidate information on the electronic structure in the liquid state. Figure 18 shows the optical reflectivity (45) of ℓ- $Au_{81}Si_{19}$(-o-o-) measured at a temperature of 420°C. For comparison the spectra of the a- $Au_{81}Si_{19}$ (full line) prepared by getter sputtering in argon (46) and of pure crystalline Au (-·-·) are also presented. The broken lines indicate the results from the Drude formula. The reflectivity of the ℓ- alloy decreases with increasing photon energy without any sharp structure. This is similar to the a-state, but the absolute values are higher by about 5-10%. The behaviour of the ℓ- and a-alloy is very different from that of pure crystalline Au which has a characteristic reflection edge at an energy of 2.4eV. However, there is a significant difference between the ℓ- and the a-alloy concerning the relaxation time and therefore the optical resistivity. This difference is directly related to the lower reflectivity of the a- compared to the ℓ-alloy. We feel that the large discrepancy between the optical and DC resistivity

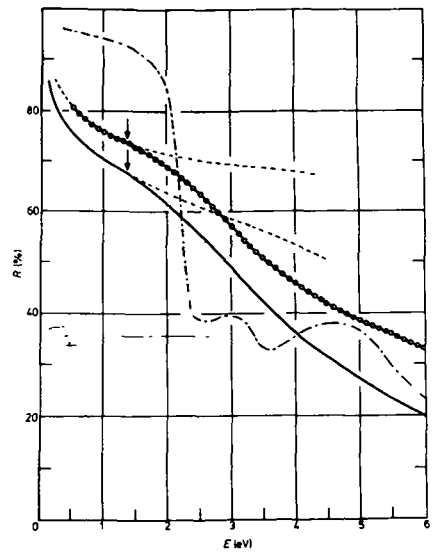

Fig.18 Optical reflectivity of liquid and amorphous $Au_{81}Si_{19}$.

in the a-state might be caused by scattering from the nonperfect surface of the a-films.

The differential optical reflectivity of several dilute liquid alloys of Au, Ag, Cu and Sn have been measured (47). The observed deviations from a simple Drude behaviour could be explained in terms of virtual bound states arising from the d-electrons of the noble metal. A detailed analysis reveals the energy of the center E_d and the width 2Δ of the virtual bound states. Figure 19 shows the concentration dependence of E_d and 2Δ for liquid Au-Sn alloys. The extrapolation of E_d and 2Δ as a function of concentration to pure Au leads to an estimate of the position and width of the d-band of pure liquid Au. These are in good agreement with the results of photoemission experiments (48). Therefore it is tempting to suppose that an extrapolation determines the position

and width of the d-states over the entire concentration range.

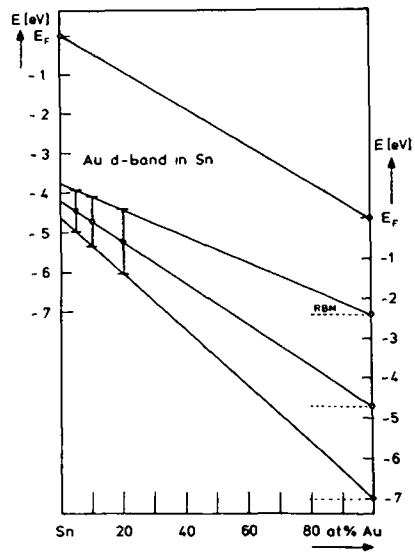

Fig.19 Position and width of the d-virtual bound states of liquid Au-Sn alloys.

ACKNOWLEDGEMENTS - We are grateful to Thomas Gabriel for skillful preparation work of the metallic glasses. Certainly, we would like to thank many of our colleagues and collaborators in the field of liquid and glassy metals for stimulating discussions. In particular, we are indebted to Prof.Dr. S.R. Nagel and Prof.Dr. R. Harris for careful reading parts of the manuscript. Financial support of the Swiss National Science Foundation, the Kommission zur Förderung der wissenschaftlichen Forschung, the Eidgenössische Stiftung zur Förderung Schweizerischer Volkswirtschaft and the Fonds für Lehre und Forschung is gratefully acknowledged.

REFERENCES

(1) A.R. Williams, J. Kübler, and C.D. Gelatt Jr., Phys.Rev. B19, 6094 (1979).

(2) B. Delley, H. Beck, H.U. Künzi and H.-J. Güntherodt, Phys.Rev. Lett. 40, 193 (1978).

(3) B. Delley, H. Beck, D. Trautmann, and F. Rösel, J.Phys. F: Metal Phys., 9, 505 (1979).

(4) B. Delley and H. Beck, J.Phys. F: Metal Phys., 9, 517 and 2231 (1979).

(5) J.C. Duthie and D.G. Pettifor, Phys. Rev. Lett., 38, 564 (1977).

(6) S.R. Nagel, Phys.Rev. B16, 1694 (1977); K. Froböse and J. Jäckle, J.Phys. F, 7, 2331 (1977); P. Cote and L. Meisel, Phys.Rev. Lett., 39, 102 (1977).

(7) G.R. Gruzalski, J.A. Gerber and D.J. Sellmyer, Phys.Rev. B19, 3469 (1979).

(8) K.H.J. Buschow, N.M. Beekmans, Phys. Rev. B19, 3843 (1979).

(9) S.R. Nagel, Proc. Conference on Metallic Glasses: Science and Technology, Budapest, Hungary (1980).

(10) R.W. Cochrane, R. Harris, J.O. Strom-Olson, and M.J. Zuckerman, Phys.Rev. Lett. 35, 676 (1975).

(11) C.C. Tsuei, Solid State Com. 27, 691 (1978).

(12) N.F. Mott, Philos. Mag. 26, 1249 (1972).

(13) F. Brouers, J. de Physique 39, L323 (1978).

(14) M. Jonson and S. Girvin, Phys.Rev. Lett. 43, 1447 (1979).

(15) J.H. Mooij, Phys. Status Solidi A17, 521 (1973).

(16) J.P. Carini, S. Basak and S.R. Nagel, these proceedings.

(17) N.F. Mott, Philos. Mag. 38, 549 (1978).

(18) L.E. Ballentine and M. Huberman, J., J.Phys. C: Solid St. Phys. 10, 4991 (1977).

(19) L.E. Ballentine and M. Huberman, J. Phys. C: Solid St. Phys. 13, 2331 (1980).

(20) G. Busch and H.-J. Güntherodt, Solid State Physics 29, 235 (1974).

(21) S.R. Nagel, G.B. Fischer and J. Tauc, Phys.Rev. B13, 3284 (1976).

(22) P. Oelhafen, M. Liard, H.J. Güntherodt, K. Berresheim and H.D. Polaschegg, Solid St. Com. 30, 641 (1979).

(23) J.D. Riley, L. Ley, J. Azoulay and K. Terakura, Phys.Rev. B20, 776 (1979).

(24) B.J. Waclawski and D.S. Boudreaux, Solid St. Com. 33, 589 (1980).

(25) E. Cartier, Y. Baer, M. Liard and H.J. Güntherodt, J.Phys. F: Metal Phys. 10, L21 (1980).

(26) M. Matsuura, T. Namoto, F. Itoh and K. Suzuki, Sol. State Com. 33, 895 (1980).

(27) P. Oelhafen et al., to be published.

(28) S.R. Nagel, J. Tauc and B.C. Giessen, Solid St. Com. 22, 471 (1977).

(29) A. Amamou and G. Krill, Solid St. Com. 28, 957 (1978).

(30) P. Oelhafen, E. Hauser, H.J. Güntherodt and K.H. Bennemann, Phys. Rev. Lett. 43, 1134 (1979).

(31) A. Amamou, Solid St. Com. 33, 1029 (1980).

(32) P. Oelhafen, E. Hauser and H.-J. Güntherodt, Solid St. Com. (1980).

(33) S. Hüfner, G.K. Wertheim, and J.H. Wernick, Phys.Rev. 8, 4511 (1973).

(34) F.L. Battye, H. Schulz, A. Goldmann, S. Hüfner, D. Seipler, and B. Elschner, J.Phys. F: Metal Phys. 8, 709 (1978).

(35) J. Kübler, K.H. Bennemann, P. Oelhafen, R. Lapka, F. Rösel and H.J. Güntherodt, to be published.

(36) A.R. Williams, C.D. Gelatt,Jr. and V.L. Moruzzi, private communication.

(37) W.M. Temmerman, R.H. Fairlie and B.L. Gyorffy, these proceedings.

(38) B. Delley, D.E. Ellis and A.J. Freeman, these proceedings.

(39) C.F. Hague, W.M. Temmermann, P. Oelhafen and H.-J. Güntherodt, to be published.

(40) P.J. Durham, D. Ghaleb, B.L. Györffy, C.F. Hague, J.-M. Mariot, G.M. Stocks, and W. Temmermann, J.Phys. F: Metal Phys. 9. 1719 (1979).

(41) S. Svensson et al., J. of Electron Spec. 9, 51 (1976).

(42) M.S. Chung, T.E. Everhart, Phys.Rev. B15, 4699 (1977).

(43) J. Hölzl, F.K. Schulte, in Springer Tracts in Modern Physics, Vol.85 (1979).

(44) A. Schlegel, P. Wachter, K.P. Ackermann, M. Liard and H.-J. Güntherodt, Solid St. Com. 31, 373 (1979).

(45) K.P. Ackermann, M. Liard and H.-J. Güntherodt, J.Phys. F: Metal Phys. 10, L51 (1980).

(46) E. Hauser, R.J. Zirke, J. Tauc, J.J. Hauser and S.R. Nagel, Phys.Rev. Lett. 40, 1733 (1978), Phys.Rev. B19, 6331 (1979).

(47) K.P. Ackermann and H.-J. Güntherodt, J.Phys. F: Metal Phys. (1980).

(48) D.E. Eastman, Phys.Rev. Lett. 26, 1108 (1971).